J. Fluid Mech. (1986), *vol.* 166, *pp.* 245–264
Printed in Great Britain

Thermocapillary and centrifugal-buoyancy-driven motion in a rapidly rotating liquid cylinder

By MARC K. SMITH
Department of Mechanical Engineering, The Johns Hopkins University, Baltimore, Maryland 21218

(Received 30 May 1984 and in revised form 9 September 1985)

The thermocapillary flow field in a uniformly rotating liquid cylinder heated from above is calculated using linear boundary-layer theory appropriate for small values of the Ekman number. The results show that the thermocapillary flow is confined to a thin layer at the liquid–gas interface if the temperature difference across the cylinder is sufficiently small. The interior flow is a uniform rotation with the endplates.

The flow due to centrifugal buoyancy is also analysed using the same theory. The magnitude of this flow compared with the thermocapillary motion is small in typical circumstances. However, it does influence the temperature field in the interior of the cylinder, whereas the thermocapillary motion does not. Full details of these flows and the first-order corrections to the interface shape are presented.

1. Introduction

Buoyancy-driven convection can be a major physical limitation in many materials-processing techniques. Thus one can see why the Space Shuttle's ability to deliver a true microgravity environment for an extended period of time has simulated a large amount of interest and research in those techniques which would benefit from such an environment. One of these techniques is the float-zone processing of single crystals from the melt. In this paper we shall describe the fluid dynamics of the melt associated with the interaction of two of the dominant mechanisms for fluid motion in this system.

The float-zone process of crystal growth from the melt is shown schematically in figure 1(*a*). Here a ring heater maintains a liquid 'float zone' that bridges the gap between two cylindrical rods. The lower polycrystalline feed rod travels into the zone, where it is melted, while the upper rod is pulled out of the zone to form a single crystal. During this process a small amount of dopant is added so that the final crystal will have certain desired electrical properties. Ideally, the dopant should be uniformly distributed throughout the crystal in both the radial and axial directions, but depending on the particular dopant–crystal combination this can be very difficult to achieve. For example, Keller & Muhlbauer (1981) show that for phosphorous-doped silicon crystals with a 53 mm diameter a total radial resistivity variation of about 15% is the best that can be achieved. Even resistivity variations as high as 60% are possible depending on the particular process parameter settings. (Here the resistivity of the crystal at any location is inversely related to the dopant concentration at that location.)

Two of the major factors affecting the dopant distribution in the crystal are the flow field and the temperature field in the melt. These fields influence the crystal-growth

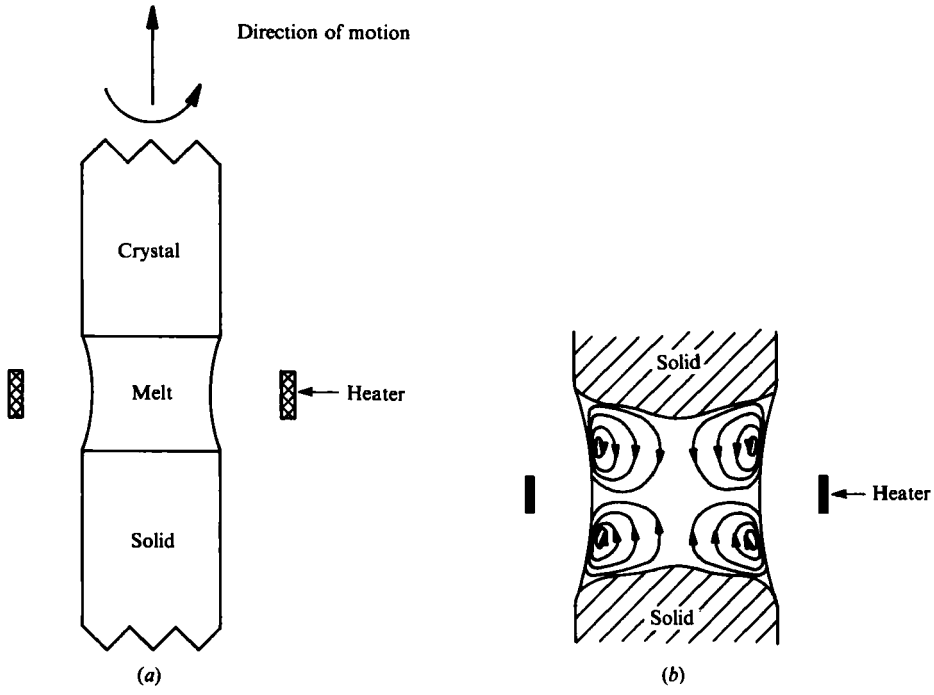

FIGURE 1. Sketches of (*a*) the geometry of the float-zone crystal-growth technique, and (*b*) the typical thermocapillary convection cells seen in a float zone (from Schwabe *et al.* 1978).

process in two ways. First, they can affect the shape of the crystallizing interface, which in turn can affect the radial dopant concentration. Secondly, the flow field can modify the thickness of the diffusion boundary layer of dopant-rich liquid that forms near the crystallizing interface as a result of the segregation of dopant during crystallization. This thickness modification then affects the concentration of the dopant incorporated into the crystal. Thus a complete understanding of these fields and their interaction with the crystallization process is necessary in order to truly optimize the float-zone crystal-growth technique.

The first step in such an understanding is to investigate the types of fluid motion present in a float zone without crystal growth. There are several driving forces present. The crystal and the feed rod can be rotated either independently or together to produce a forced convection in the zone. The non-uniform temperature field induced by the heater will produce variations in the density of the melt which cause fluid motion through the vertical gravitational force or the radial centrifugal force if the float zone is rotating. The non-uniform temperature field will also produce variations in the surface tension of the melt–gas interface which cause a fluid motion known as thermocapillary convection. In general, these motions cannot be studied independently because they are intimately coupled. However, in this paper we are interested in the float-zone processing of single crystals in the *microgravity* environment of Space, and so we can safely neglect gravitationally driven buoyancy flows.

Of the remaining flows mentioned, thermocapillary convection in a float zone *without rotation* has been studied extensively both numerically and experimentally (for a review of this work see Schwabe 1981). The main characteristics of such flows are shown in figure 1 (*b*). Here we see two toroidal convection cells whose centres lie

close to the melt–gas interface but which penetrate completely into the interior of the zone. The experimental work of Chun (1980) and the numerical work of Kobayashi (1984) have suggested that these cells become confined to a thin region near the melt–gas interface if the zone is uniformly rotated with a large enough angular velocity. In this work, we perform the detailed calculations which describe the flow in this limit.

To begin we simplify the float-zone geometry to that of an axisymmetric shape in uniform rotation. The governing equations are properly scaled and presented in §2. The first assumption made is that of large surface tension and of a particular liquid volume so that the free surface assumes the shape of a circular cylinder which behaves to first order as a non-deformable surface, but one that is able to support thermocapillary stresses. This greatly simplifies the free-surface boundary conditions. One of the parameters derived from the scaling of the equations is the Ekman number E defined as the ratio of the viscous forces to the Coriolis forces in the zone. For a silicon float zone one centimetre in radius rotating at one radian per second $E = 0.0035$. With such a small value of E one may suspect the existence of viscous boundary layers as described by Greenspan (1968) for various other rotating systems. An analytical representation of these boundary layers is presented in §3 under the additional assumption that the axial velocity at the liquid–gas interface (or equivalently the temperature difference across the zone) is small enough so that the nonlinear terms in the governing equations can be neglected.

For completeness, we consider the remaining buoyancy-driven motion caused by the radial centrifugal force field in §4. To distinguish this from the gravitationally driven flows seen in Earth-based processes we call this a centrifugal-buoyancy-driven motion. Such flows in rigid cylinders have been well studied by Barcilon & Pedlosky (1967) and by Homsy & Hudson (1969). As we shall see, the free surface in this work has a distinct effect on the motion in the boundary layer that appears along the side. Also, in §5 we calculate the effect of the centrifugal-buoyancy flow on the temperature field in the interior of the cylinder.

Section 6 shows how the free surface of the liquid is deformed from its original cylindrical shape as a result of the above flows. This deformation is calculated as the next term in a perturbation series for small capillary number, i.e. for large surface tension.

Finally, since our original motivation for studying this problem has to do with crystal growth, we discuss the restrictions placed upon the operating parameters as a result of the linear assumption for a float zone of silicon, one of the most common materials used in this process.

2. Formulation

The float-zone geometry used in this investigation is shown in figure 2. It is described using a cylindrical coordinate system (r, θ, z), with unit vectors $(\boldsymbol{e}_r, \boldsymbol{e}_\theta, \boldsymbol{e}_z)$, and whose origin lies in the centre of the zone. The z-axis lies along the axis of symmetry of the zone. The top and bottom of the zone are rigid plates located at $z = \pm L$. The lateral interface between the liquid and the ambient gas is located at $r = \eta(z)$ and is assumed to be both slightly deformable and able to support thermocapillary stresses.

The liquid zone and the top and bottom plates are uniformly rotating at the constant angular velocity $\boldsymbol{\omega} = \Omega \boldsymbol{e}_z$. The top and bottom plates are held at the constant temperatures T_H and T_C respectively, with $T_H > T_C$. Outside the zone the

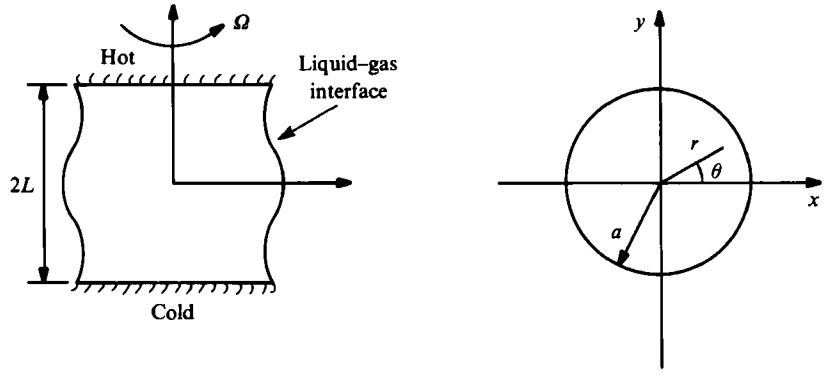

FIGURE 2. The axisymmetric float-zone geometry.

ambient gas is assumed to be passive with a constant pressure and a temperature T_a that varies linearly from T_H at the top of the zone to T_C at the bottom. Gravity is ignored.

The velocity in the liquid is $\boldsymbol{v} = (u, v, w)$, P the pressure, T the temperature, ρ the fluid density, μ the viscosity, σ the surface tension, γ_T the negative rate of change of surface tension with temperature, β the thermal expansion coefficient, κ the thermal diffusivity, k the thermal conductivity, and h is the thermal unit-surface conductance.

The equation of state for the surface tension is assumed to be $\sigma = \sigma_0 - \gamma_T(T - T_0)$ where T_0 is a reference temperature and σ_0 is the surface tension at that temperature. The density is assumed to be $\rho = \rho_0[1 - \beta(T - T_0)]$, where ρ_0 is the density at $T = T_0$.

The governing equations are scaled as follows: a, radial length; L, axial length; U_s, axial velocity; $U_s a/L$, radial and azimuthal velocity; $\rho_0 U_s \Omega a$, pressure; $\Delta T = \frac{1}{2}(T_H - T_C)$, temperature; and $T_0 = \frac{1}{2}(T_H + T_C)$, reference temperature. The velocity scale U_s is actually the axial interfacial velocity at the liquid–gas interface due to thermocapillarity and is unknown at this point. These scales give rise to the following dimensionless parameters: the aspect ratio $A \equiv a/L$; the Ekman number $E \equiv \nu/\Omega a^2$; the Rossby number $\epsilon \equiv U_s/\Omega a$; the buoyancy number $\alpha \equiv \beta \Delta T/\epsilon$; the Prandtl number $Pr \equiv \nu/\kappa$; the ratio of the surface-tension gradient to viscous forces $M_T \equiv \gamma_T \Delta T/\mu U_s$; the capillary number $Ca \equiv \mu U_s/\sigma_0$; the rotational Bond number $B_\Omega \equiv \rho_0 \Omega^2 a^3/\sigma_0$; and the Biot number $B \equiv ha/k$.

The dimensionless governing equations for steady axisymmetric flow in a frame of reference rotating with the cylinder are as follows:

$$\epsilon A\left[uu_r + wu_z - \frac{v^2}{r}\right] = -A^{-1}p_r - A^{-1}\alpha r T + 2v + E\left[u_{rr} + \frac{u_r}{r} + A^2 u_{zz} - \frac{u}{r^2}\right], \quad (2.1a)$$

$$\epsilon A\left[uv_r + wv_z + \frac{uv}{r}\right] = -2u + E\left[v_{rr} + \frac{v_r}{r} + A^2 v_{zz} - \frac{v}{r^2}\right], \quad (2.1b)$$

$$\epsilon A[uw_r + ww_z] = -Ap_z + E\left[w_{rr} + \frac{w_r}{r} + A^2 w_{zz}\right], \quad (2.1c)$$

$$\epsilon A[uT_r + wT_z] = Pr^{-1}E\left[T_{rr} + \frac{T_r}{r} + A^2 T_{zz}\right], \quad (2.1d)$$

$$\frac{1}{r}\frac{\partial}{\partial r}(ru) + w_z = 0, \quad (2.1e)$$

where $$p = P - r^2/2\epsilon. \tag{2.1f}$$

The boundary conditions on the top and bottom rigid plates are

$$\boldsymbol{v} = T \mp 1 = 0. \tag{2.1g}$$

The boundary conditions on the deformable free surface are as follows: normal stress

$$-pCaE^{-1} - \tfrac{1}{2}\eta^2 B_\Omega + 2CaAN^{-2}[u_r - \eta_z(w_r + A^2 u_z) + A^2\eta_z^2 w_z] = 2H(1 - M_T\, CaT); \tag{2.1h}$$

tangential stress

$$\{A^2\eta_z[2u_r - \eta_z(w_r + A^2 u_z)] + w_r + A^2 u_z - 2A^2 w_z\,\eta_z\}\, N^{-1} = -M_T\, A(T_z + \eta_z T_r), \tag{2.1i}$$

$$v_r - \frac{v}{r} - A^2\eta_z v_z = 0; \tag{2.1j}$$

the kinematic condition $$u = \eta_z w; \tag{2.1k}$$

and the thermal condition $$(T_r - A^2\eta_z T_z)\, N^{-1} + B(T - T_a) = 0; \tag{2.1l}$$

where the curvature is

$$2H = A^2\eta_{zz} N^{-3} - (\eta N)^{-1}, \quad N = (1 + A^2\eta_z^2)^{\frac{1}{2}}, \tag{2.1m, n}$$

and the ambient temperature is $$T_a = z. \tag{2.1o}$$

To complete the boundary conditions, we shall assume that the contact lines at $z = \pm 1$ are pinned to the rigid plates so that

$$\eta = 1 \quad \text{at } z = \pm 1. \tag{2.1p}$$

In addition, the liquid volume is constant, so

$$a^2 L \int_{-1}^{1} \pi\eta^2\, \mathrm{d}z = V, \quad \text{a constant.} \tag{2.1q}$$

We choose V to be the volume of the cylinder of radius a and length $2L$, i.e. $V = 2\pi a^2 L$, so that now

$$\int_{-1}^{1} \eta^2\, \mathrm{d}z = 2. \tag{2.1r}$$

Our first simplification of these equations will be with respect to the free-surface boundary conditions. In table 1 we list typical material properties for liquid silicon at 1410 °C. For a silicon zone with $a = L = 1$ cm, rotating at the angular velocity $\Omega = 1$ rad/s, we find that $B_\Omega = 0.0035 \ll 1$. The capillary number cannot be computed at this point because U_s is unknown. However, even for $U_s = 100$ cm/s, which is an unreasonably large number for the interfacial velocity, we have $Ca = 0.0012 \ll 1$.

With both Ca and $B_\Omega \ll 1$ and the liquid volume chosen appropriately, we can assume that the liquid zone is nearly a circular cylinder. The system (2.1) can now be solved by expanding all dependent variables in a power series in Ca. Therefore

$$\eta = 1 + CaS(z) + O(Ca^2), \tag{2.2a}$$

$$p = Ca^{-1}p_{-1} + p_0 + O(Ca), \tag{2.2b}$$

$$(u, v, w, T) = (u_0, v_0, w_0, T_0) + O(Ca). \tag{2.2c}$$

Material properties	Process parameters
$\mu = 0.88\times10^{-2}$ g/(cm s)	$\Omega = 1$ rad/s
$\rho_0 = 2.5$ g/cm^3	$a = 1$ cm
$\nu = 0.35\times10^{-2}$ cm^2/s	$L = 1$ cm
$k = 0.32\times10^{7}$ erg/(s cm °C)	$A = 1$
$\kappa = 0.15$ cm^2/s	$E = 0.0035$
$\sigma_0 = 720$ dyn/cm	$B_\Omega = 0.0035$
$\gamma_T = 0.43$ dyn/(cm °C)	$A^{-1}\alpha = 0.19\times10^{-4}$
$\beta = 1.43\times10^{-4}$ °C^{-1}	$U_s = 7.4\,\Delta T$ cm/(s °C)
$Pr = 0.023$	$Ca = 9.0\times10^{-5}\Delta T$ °C^{-1}
	$\epsilon = 7.4\,\Delta T$ °C^{-1}

TABLE 1. The material properties of liquid silicon at 1410 °C, and typical process parameters for a silicon float zone

Substituting forms (2.2) into system (2.1) we find that at $O(Ca^{-1})$, p_{-1} = constant. We can determine this constant from the normal-stress boundary condition (2.1*h*), which is now

$$-p_{-1}E^{-1}-\tfrac{1}{2}B_\Omega+1+Ca\,[-p_0E^{-1}+2Au_{0r}-A^2S''-S(1+B_\Omega)]+O(Ca^2)=0. \quad (2.3)$$

Thus
$$p_{-1} = E(1-\tfrac{1}{2}B_\Omega). \quad (2.4)$$

At $O(1)$ we find that the differential equations stay exactly as given in system (2.1), and that the free-surface boundary conditions become those appropriate to a surface incapable of moving normal to itself, but able to support tangential stresses. These are

$$\left.\begin{aligned} u_0 &= 0, && (2.5a)\\ w_{0r} &= -M_T AT_{0z}, && (2.5b)\\ v_{0r}-\frac{v_0}{r} &= 0, && (2.5c)\\ T_{0r}+B(T_0-T_a) &= 0 && (2.5d) \end{aligned}\right\} \text{ on } r=1.$$

The solution of system (2.1) with the boundary conditions (2.5) will be the subject of the next three sections of this paper, and hence, for simplicity, we shall drop the zero subscript.

We shall solve these equations in terms of a stream function defined as

$$w = -\frac{1}{r}\frac{\partial}{\partial r}(r\psi), \quad u = \psi_z. \quad (2.6a,b)$$

The global mass-conservation condition is

$$\psi = 0 \quad \text{on } r=1 \quad \text{and} \quad z=\pm1. \quad (2.6c)$$

3. The thermocapillary flow

To solve the system of equations (2.1) with boundary conditions (2.5) we first assume that ϵA is small enough so that the nonlinear terms can be ignored. The resulting linear system is then solved in two parts: one due to thermocapillarity and one due to centrifugal buoyancy.

The flow due to thermocapillarity is described by (2.1) with $\epsilon A = \alpha = 0$. For the

typical silicon zone described in table 1, $E = 0.0035$. Thus we expect boundary-layer behaviour on all surfaces and a core flow in which viscous effects are small. To solve for this core flow we drop the two viscous boundary conditions on the liquid–gas interface and note that the temperature field has now decoupled from the velocity field. Since this coupling provides the only mechanism for fluid motion, the core solution of the linear momentum equations is just $\psi = v = p = 0$. With no motion in the core the temperature field is governed completely by conduction and can be found for any given temperature field in the ambient gas $T_a(z)$. The resulting surface temperature distribution will then force the boundary-layer flow at the liquid–gas interface through the axial viscous-stress boundary condition in (2.5*b*). Only to the next order in the small parameter ϵA is it possible for the convection field in the cylinder to influence the temperature field. For simplicity, we choose $T_a = z$. The solution for the temperature field is then also $T = z$.

Using a general scaling analysis of the linear equations (2.1), we find that the boundary layer has a lengthscale $O(E^{\frac{1}{3}})$ and that $v = O(1)$ and $\psi = O(E^{\frac{1}{3}})$. In addition, Ekman layers with a lengthscale $O(E^{\frac{1}{2}})$ appear at the rigid plates in the $E^{\frac{1}{3}}$ side layer. Instead of solving for the flow in the Ekman layers explicitly, we use the equivalent Ekman matching condition obtained from Greenspan (1968):

$$w = \mp\tfrac{1}{2}AE^{\frac{1}{2}}\frac{1}{r}\frac{\partial}{\partial r}(rv)+O(E) \quad \text{on } z = \pm 1. \tag{3.1}$$

To solve for the flow in the boundary layer at the liquid–gas interface we introduce a boundary-layer coordinate

$$\rho = (1-r)\,E^{-\frac{1}{3}}, \tag{3.2}$$

and scale

$$v = v^0, \quad \psi = E^{\frac{1}{3}}\psi^0, \tag{3.3a,b}$$

where v^0 and ψ^0 are $O(1)$ quantities. These are substituted into the governing linear system of equations (2.1) to obtain the following boundary-layer equations:

$$\psi^0_{\rho\rho\rho\rho}+2A^2v^0_z-2E^{\frac{1}{3}}\psi^0_{\rho\rho\rho}+O(E^{\frac{2}{3}}) = 0, \tag{3.4a}$$

$$v^0_{\rho\rho}-2\psi^0_z-E^{\frac{1}{3}}v^0_\rho+O(E^{\frac{2}{3}}) = 0, \tag{3.4b}$$

$$\left.\begin{aligned} \psi^0_{\rho\rho}-1-E^{\frac{1}{3}}\psi^0_\rho+O(E^{\frac{2}{3}}) &= 0, \\ v^0_\rho+E^{\frac{1}{3}}v^0+O(E^{\frac{2}{3}}) &= 0, \\ \psi^0 &= 0 \end{aligned}\right\} \quad \text{on } \rho = 0, \tag{3.4c,d,e}$$

$$\psi^0, v^0 \to 0 \quad \text{as } \rho \to \infty \tag{3.4f}$$

$$\psi^0_\rho \mp \tfrac{1}{2}AE^{\frac{1}{3}}v^0_\rho - E^{\frac{1}{3}}\psi^0 \pm \tfrac{1}{2}AE^{\frac{1}{3}}v^0+O(E^{\frac{2}{3}}) = 0 \quad \text{on } z = \pm 1. \tag{3.4g}$$

The condition (3.4*f*) is the appropriate matching condition to the stagnant core in the uniformly rotating reference frame, and condition (3.4*g*) is the equivalent Ekman matching condition.

The driving force for the motion in this boundary layer is the thermocapillary shear stress. To reflect this fact, we have chosen the velocity scale so that the thermocapillary shear stress and the fluid shear stress at the cylindrical surface are both unity, i.e. we have set $M_T AE^{\frac{1}{3}} = 1$ in developing the boundary condition (3.4*c*). The velocity scale is then defined as

$$U_s = \frac{\gamma_T \Delta T}{\mu} E^{\frac{1}{3}}A. \tag{3.5}$$

A solution of system (3.4) that is uniformly valid in terms of the boundary-layer coordinate ρ can be obtained by using the method of multiple scales. To begin we define two additional variables as follows:

$$\xi = E^{\frac{1}{6}}\rho, \quad x = E^{\frac{1}{3}}\rho = 1-r. \tag{3.6a,b}$$

We consider v^0 and ψ^0 to be functions of all the independent variables ρ, ξ, x and z, so that $\partial/\partial\rho$ becomes $\partial/\partial\rho + E^{\frac{1}{6}}\partial/\partial\xi + E^{\frac{1}{3}}\partial/\partial x$. The solution of system (3.4) is then found in terms of the following asymptotic series:

$$\psi^0 = {}^0\psi^0 + E^{\frac{1}{6}}{}^1\psi^0 + E^{\frac{1}{3}}{}^2\psi^0 + \ldots, \quad v^0 = {}^0v^0 + E^{\frac{1}{6}}{}^1v^0 + E^{\frac{1}{3}}{}^2v^0 + \ldots. \tag{3.7a,b}$$

From this analysis a leading-order approximation for the flow in the cylinder that is uniformly valid in the coordinate ρ is given as

$$\psi = E^{\frac{1}{3}} \sum_{n=1}^{\infty} f^{(n)}(\rho, \xi, x) \cos\lambda_n z + \ldots, \tag{3.8a}$$

$$v = -\frac{1}{2A^2} \sum_{n=1}^{\infty} \frac{\partial^4 f^{(n)}}{\partial\rho^4}(\rho, \xi, x) \frac{\sin\lambda_n z}{\lambda_n} + \ldots, \tag{3.8b}$$

$$f^{(n)}(\rho, \xi, x) = \frac{4A}{\sqrt{3}} \frac{(-1)^{n+1}}{\gamma_n^5} \exp(\tfrac{1}{2}x) \left\{ \frac{\sqrt{3}}{2} \exp\left(-\gamma_n\rho - \frac{A}{3\gamma_n}\xi\right) + \exp\left(-\tfrac{1}{2}\gamma_n\rho - \frac{A}{6\gamma_n}\xi\right) \sin\left[\frac{\sqrt{3}}{2}\gamma_n\rho - \frac{A}{2\sqrt{3}\gamma_n}\xi - \frac{2\pi}{3}\right] \right\}, \tag{3.8c}$$

$$\lambda_n = (n-\tfrac{1}{2})\pi, \tag{3.8d}$$

$$\gamma_n = (2A\lambda_n)^{\frac{1}{3}}. \tag{3.8e}$$

In figures 3(*a*) and (*b*) we show the meridional circulation and the azimuthal velocity respectively for $A = 1$ and $E = 10^{-6}$. A particular value of the Ekman number is chosen here because E appears implicitly in the leading-order approximation of the solution through the scaled variables ξ and x. This is typical of asymptotic solutions obtained by the method of multiple scales. These figures extend from the interface to about 4 % of the cylinder radius for this value of E. Note that the 'cellular' behaviour seen in figure 3(*a*) continues into the interior but with a magnitude that decays exponentially like $\exp(-\frac{1}{2}\gamma_1 E^{-\frac{1}{3}}(1-r))$. Figures 3(*c*) and (*d*) show how the motion in the layer is deformed as the Ekman number is increased from 10^{-6} to 10^{-3}. However, note that when $E = 10^{-3}$ the extent of the figures is 40 % of the cylinder radius.

The flow field in the cylinder is relatively simple because of the decoupling of the driving force at the liquid–gas interface from the interior fluid. The thermocapillary stress at this interface is balanced by viscous stresses in a boundary layer with an $O(E^{\frac{1}{3}})$ lengthscale. As one moves away from the interface, viscous stresses cannot balance the resultant Coriolis forces and so the interior of the cylinder remains motionless. This confinement of the thermocapillary convection to a boundary layer at the liquid–gas interface is a consequence of the Taylor–Proudman theorem for the motion in the inviscid core, since such motion cannot vary in the z-direction.

The azimuthal velocity in the boundary layer is an odd function of z and is not zero on either the top or bottom plates, as shown in figure 3(*b*). These rigid-plate boundary conditions are satisfied in Ekman layers with a lengthscale $O(E^{\frac{1}{3}})$. The upper Ekman layer produces a net mass flux out of the top edge of the $E^{\frac{1}{3}}$ layer which is ejected back into the side layer by an $E^{\frac{1}{3}}$ by $E^{\frac{1}{3}}$ corner source singularity located

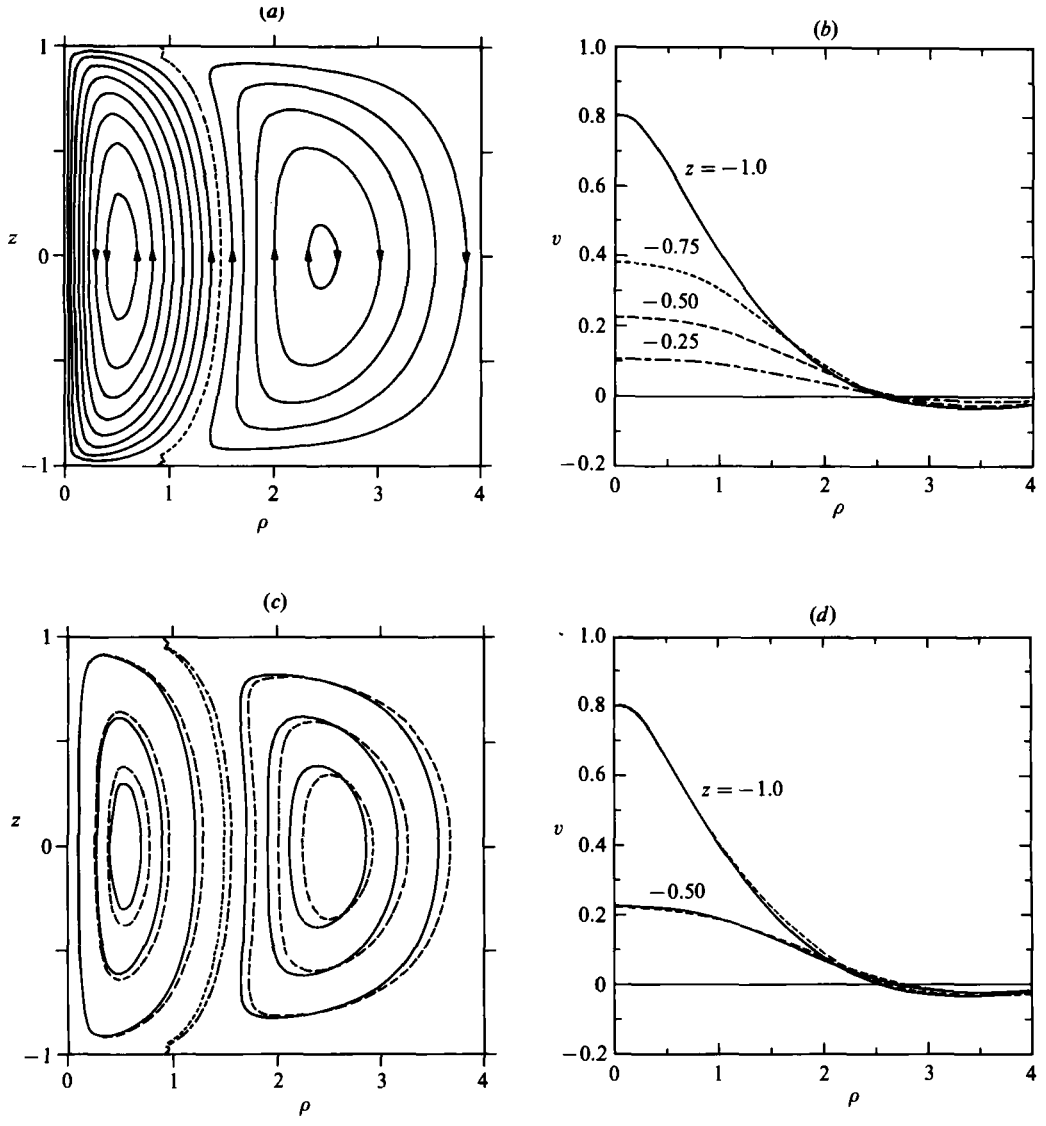

FIGURE 3. Thermocapillary motion in the side boundary layer of the liquid cylinder with $A = 1$. (*a*) The meridional circulation for $E = 10^{-6}$; the kinks in the zero streamline (dotted line) are an artifact of the plotter. (*b*) The azimuthal velocity for $E = 10^{-6}$: ——, $z = -1.0$; – – – –, -0.75; — — —, -0.5; — — — — —, -0.25. (*c*) A comparison of the meridional circulation for $E = 10^{-6}$ (——) and $E = 10^{-3}$ (— — —). (*d*) A comparison of the azimuthal velocity at $z = -1.0$ and $z = -0.5$ for $E = 10^{-6}$ (——) and $E = 10^{-3}$ (— — —).

at $z = 1$, $r = 1$. Similarly, the lower Ekman layer produces a net mass flux into the $E^{\frac{1}{3}}$ layer along its bottom edge. An $E^{\frac{1}{3}}$ by $E^{\frac{1}{3}}$ corner sink singularity located at $z = -1$, $r = 1$ feeds the required mass to this Ekman layer from the convection field in the side layer. The resultant flow is a small correction to the leading-order convection field in the side layer. The multiscale analysis used to obtain the leading- order stream function (3.8*a*) also gives us most of this first-order correction. We shall assume the same x-variation as in the leading-order term, i.e. $e^{\frac{1}{2}x}$, because of the difficulty of the analysis at the order needed to obtain the x-variation directly. The meridional

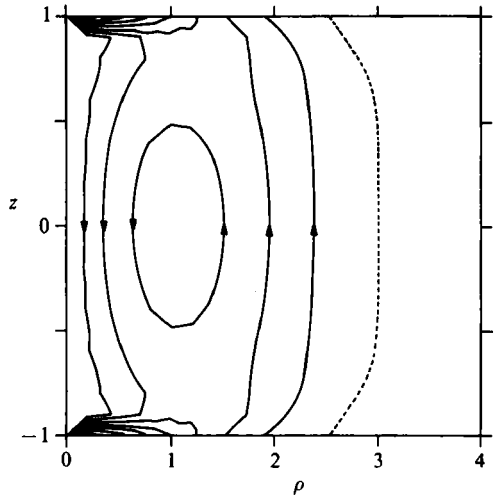

FIGURE 4. The first-order correction to the thermocapillary meridional circulation in the side boundary layer of the liquid cylinder with $A = 1$ and $E = 10^{-6}$.

circulation for the correction is shown in figure 4 for $E = 10^{-6}$ and $A = 1$. Our x-variation assumption amounts to a difference of about 2% at $\rho = 4$ for the given parameter values with respect to no x-variation. Note that this flow is not a uniform correction to the leading-order convection field of figure 3(a) because of the appearance of the corner singularities.

Hunter (1967) discussed in detail how this correction in the side layer is obtained. Even though he studied the flow due to buoyancy in a heated annulus with rigid sidewalls and did not use a multiscale method, the essential details of the interaction of the flow in the side layer with the Ekman layers at the top and bottom are the same. However, Hunter's correction is not uniformly valid in the radial coordinate, which is why a multiscale analysis was used in the present work.

4. The centrifugal buoyancy flow

System (2.1) and the boundary conditions (2.5) with $\epsilon A = M_T = 0$ describe the linear theory for the motion in the liquid cylinder due to centrifugal buoyancy. Since the Ekman number is small the motion in the cylinder is composed of four parts: a core motion, an Ekman layer on the top and the bottom plates, and a side layer on the liquid–gas interface. The effect of the Ekman layers on the core is described by the equivalent Ekman matching conditions (3.1), and so the motion in these boundary layers will not be calculated explicitly.

The solution in the core is given by an expansion in powers of $E^{\frac{1}{2}}$ as follows:

$$\hat{u} = O(E), \quad \hat{v} = \tfrac{1}{2}A^{-1}\alpha r z + O(E^{\frac{1}{2}}), \quad \hat{w} = -\tfrac{1}{2}\alpha E^{\frac{1}{2}} + O(E), \qquad (4.1a,b,c)$$

$$\hat{p} = \hat{p}^1(r)\,E^{\frac{1}{2}} + O(E), \quad \hat{\psi} = \tfrac{1}{4}\alpha r E^{\frac{1}{2}} + O(E), \quad T = z, \qquad (4.1d,e,f)$$

where the 'hat' refers to core variables. This solution satisfies all the boundary conditions at the liquid–gas interface *to leading order in the small parameter* E except for the stream-function condition. Thus a boundary layer forms at this interface in order to transfer mass from the lower Ekman layer to the upper. Note also that the effects of convection on the temperature profile, which include boundary-layer

behaviour at the liquid–gas interface, come in to the next order in the small parameter ϵA.

To investigate the flow in the side layer we introduce a boundary-layer coordinate defined as in (3.2) and scale the dependent variables as

$$v = E^{\frac{1}{3}}\bar{v}^0, \quad \psi = E^{\frac{1}{2}}\bar{\psi}^0. \tag{4.2a,b}$$

The resulting boundary-layer equations are the same as for the thermocapillary problem, but with different boundary conditions on the surface of the cylinder, i.e.

$$\left.\begin{aligned} \bar{\psi}^0_{\rho\rho} - E^{\frac{1}{3}}\bar{\psi}^0_{\rho} + O(E^{\frac{2}{3}}) &= 0, && (4.3a)\\ \bar{v}^0_{\rho} + E^{\frac{1}{3}}\bar{v}^0 + O(E^{\frac{2}{3}}) &= 0, && (4.3b)\\ \bar{\psi}^0 &= -\tfrac{1}{4}\alpha + O(E^{\frac{1}{3}}) && (4.3c) \end{aligned}\right\} \quad \text{on } \rho = 0.$$

This system of equations can be solved using the method of multiple scales in exactly the same manner as for the thermocapillary problem. The resulting approximation for the flow due to centrifugal buoyancy uniformly valid in the coordinate r is

$$\psi = E^{\frac{1}{2}}\left[\tfrac{1}{4}\alpha r + \sum_{n=1}^{\infty} \bar{f}^{(n)}(\rho, \xi, x)\cos\lambda_n z\right] + \ldots, \tag{4.4a}$$

$$v = \tfrac{1}{2}A^{-1}\alpha r z - \frac{E^{\frac{1}{3}}}{2A^2}\sum_{n=1}^{\infty}\frac{\partial^4 \bar{f}^{(n)}}{\partial\rho^4}\frac{\sin\lambda_n z}{\lambda_n} + \ldots, \tag{4.4b}$$

$$\bar{f}^{(n)}(\rho, \xi, x) = -\frac{\alpha}{\sqrt{3}}\frac{(-1)^{n+1}}{\lambda_n}\exp\left(-\tfrac{1}{2}\gamma_n\rho - \frac{A}{6\gamma_n}\xi + \tfrac{1}{2}x\right) \times \sin\left[\frac{\sqrt{3}}{2}\gamma_n\rho - \frac{A}{2\sqrt{3}\gamma_n}\xi + \frac{2\pi}{3}\right], \tag{4.4c}$$

$$\lambda_n = (n - \tfrac{1}{2})\pi, \quad \gamma_n = (2A\lambda_n)^{\frac{1}{3}}. \tag{4.4d,e}$$

The meridional circulation for this problem is shown in figures 5(*a*, *b*) and the azimuthal velocity in the boundary layer is shown in figure 5(*c*) for $E = 10^{-6}$ and $A = 1$.

The centrifugal body force driving this flow is felt throughout the entire cylinder. Thus the resultant motion is not confined exclusively to a boundary layer at the liquid–gas interface as in the case of the thermocapillary flow. In the interior a swirling shear flow develops that balances centrifugal buoyancy with Coriolis forces. This non-zero azimuthal velocity is brought to zero on the top and bottom rigid plates by standard Ekman layers with also produce the constant downward axial velocity in the core. The circulation in the cylinder between the top and bottom Ekman layers is then completed by an $O(E^{\frac{1}{3}})$ mass flux in the side layer.

An analysis of the motion caused by centrifugal buoyancy in a *rigid* cylinder was done by Barcilon & Pedlosky (1967), who also included gravity, and by Homsy & Hudson (1969), who did not. The core motion, the motion in the top and bottom Ekman layers, and even the scaling of the side layer, are exactly the same as in the present problem. However, in a rigid cylinder a closed $O(E^{\frac{1}{3}})$ meridional circulation develops in the side layer so that the appropriate rigid-wall boundary conditions can be satisfied. This flow is missing in the liquid cylinder because of the stress-free sidewall.

Hunter (1967) also calculated this closed $O(E^{\frac{1}{3}})$ meridional circulation, but in the slightly different problem of a horizontally heated, rotating annulus. The boundary-

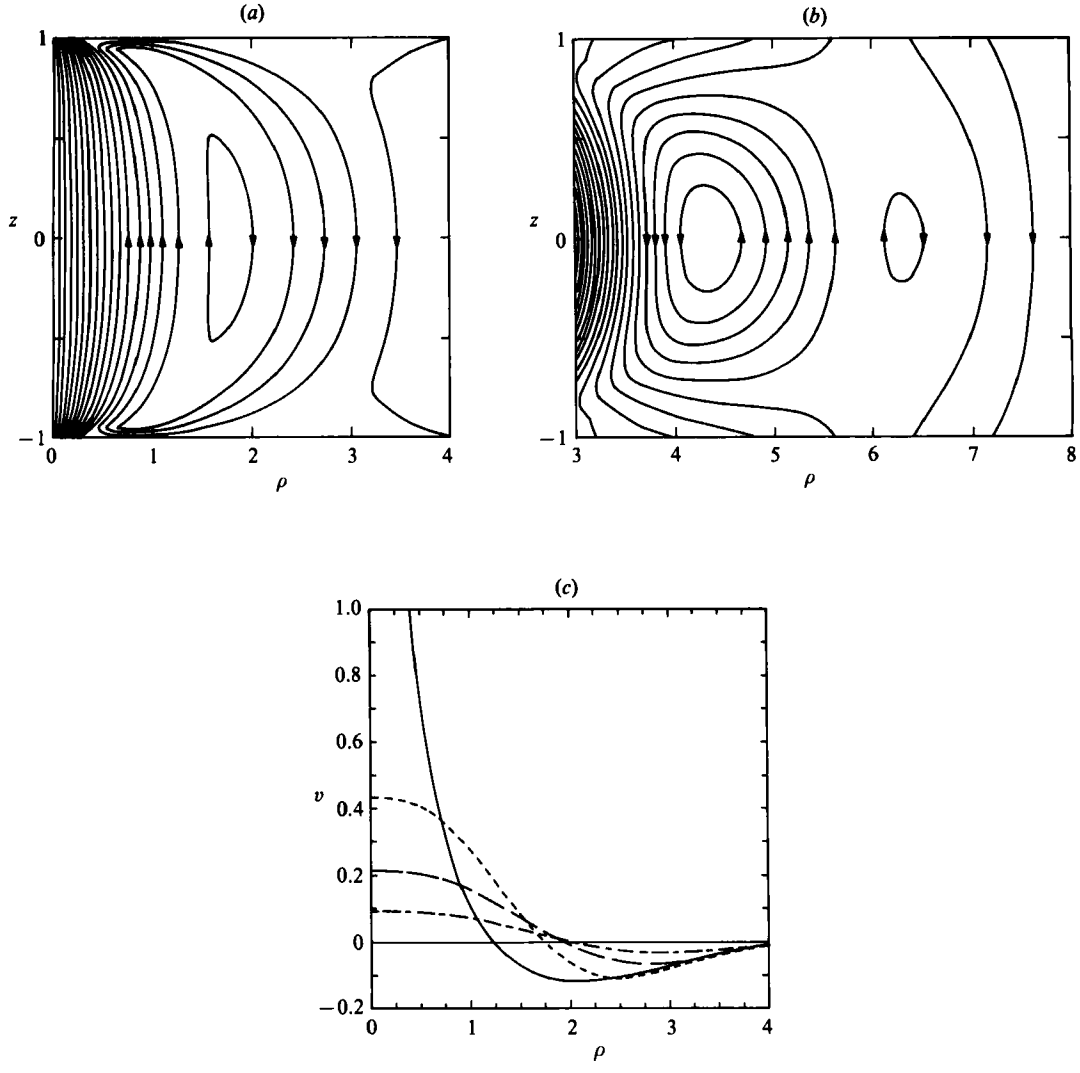

FIGURE 5. The motion in the side boundary layer due to centrifugal buoyancy with $A = 1$ and $E = 10^{-6}$. The meridional circulation is shown in (*a*) for $\rho = 0$ to $\rho = 4.0$, and in (*b*) for $\rho = 3.0$ to $\rho = 8.0$. (*c*) Azimuthal velocity: ——, $z = -1.0$; – – – –, -0.75; — — —, -0.5; — – — – —, -0.25.

layer analysis used in that problem, which he discussed in detail, is essentially the same as in the present case except for differences associated with the stress-free sidewall boundary conditions.

5. The temperature correction in the core

Of particular interest is the nonlinear correction to the linear temperature profile in the core due to the buoyancy-driven and the surface-tension-driven flows. This can be obtained from (2.1*d*, *g*) and (2.5*d*) by solving for the temperature in terms of a power series in ϵA as follows:

$$T = T^0 + \epsilon A T^1 + \ldots. \tag{5.1}$$

To leading order with the ambient temperature $T_a = z$ we find that $T^0 = z$ as before.

At the next order in ϵA we obtain a partial differential equation for T^1 that is solved in four parts: in the core, in the boundary layer at $r = 1$ and in the boundary layers at $z = \pm 1$. Since we are primarily interested in the core temperature, we solve for the temperature in the boundary layers only in order to derive an equivalent boundary condition for the core. From this analysis we obtain the following system:

$$T^1_{rr} + \frac{1}{r} T^1_r + A^2 T^1_{zz} = -\tfrac{1}{2}\alpha Pr E^{-\frac{1}{2}} + O(1), \tag{5.2a}$$

$$T^1 = O(E^{\frac{1}{2}}) \qquad \text{on } z = \pm 1, \tag{5.2b}$$

$$T^1_r + BT^1 = -\tfrac{1}{4}\alpha Pr E^{-\frac{1}{2}} + O(E^{-\frac{1}{2}}) \quad \text{on } r = 1. \tag{5.2c}$$

Note that the temperature correction described by system (5.2) is only the result of the motion due to centrifugal buoyancy. The thermocapillary convection in the boundary layer at the free surface induces no interior motion to contribute to (5.2*a*), and it does not contribute a heat flux to the equivalent core boundary condition (5.2*c*).

System (5.2) is solved in terms of a power series in $E^{-\frac{1}{3}}$, i.e.

$$T^1 = E^{-\frac{1}{3}} {}^0T^1 + E^{-\frac{1}{3}} {}^1T^1 + \ldots. \tag{5.3}$$

Thus the leading-order approximation to system (5.2) is simply

$${}^0T^1 = -\alpha Pr A^{-2}\left[\tfrac{1}{4}(z^2-1) + \sum_{n=1}^{\infty} D_n I_0(A\lambda_n r)\cos\lambda_n z\right], \tag{5.4a}$$

where

$$D_n = \frac{(-1)^{n+1}A}{2\lambda_n^2 I_1(A\lambda_n)}\left[\frac{1+\dfrac{2B}{A^2\lambda_n^2}}{1+\dfrac{BI_0(A\lambda_n)}{A\lambda_n I_1(A\lambda_n)}}\right], \tag{5.4b}$$

$$\lambda_n = (n-\tfrac{1}{2})\pi, \tag{5.4c}$$

and I_0 and I_1 are modified Bessel functions. The isotherms calculated by this analysis are shown in figure 6 for two values of the Biot number.

The net mass flux in the $E^{\frac{1}{3}}$ side layer due to centrifugal buoyancy is directed from the lower to the upper Ekman layer. This motion brings cooler fluid from the bottom of the cylinder to the warmer upper part, producing a convective cooling on the fluid in the core. The lateral boundary condition (5.2*c*) for the temperature correction in the core models this effect as an imposed *positive heat flux out of the core.*

The downward axial velocity in the interior brings warm fluid from the top of the cylinder to the cooler regions below, producing a convective heating of the fluid in the core. This effect is modelled as the *positive* rate of internal heat generation density term that appears in (5.2*a*). Note that the total rate of internal heat generation in the cylinder exactly balances the imposed heat flux out of the cylinder. This is because the buoyancy-driven convection is closed and the motion of fluid in the top and bottom Ekman layers is along constant-temperature surfaces thus producing no net heat flux into the interior.

A useful measure of the effects of convection is the total heat flux *into* either end of the cylinder, denoted by Q. In dimensionless terms this is a Nusselt number

$$Nu = \pm 2 \int_0^1 \left.\frac{\partial T}{\partial z}\right|_{z=\pm 1} r\,\mathrm{d}r, \tag{5.5a}$$

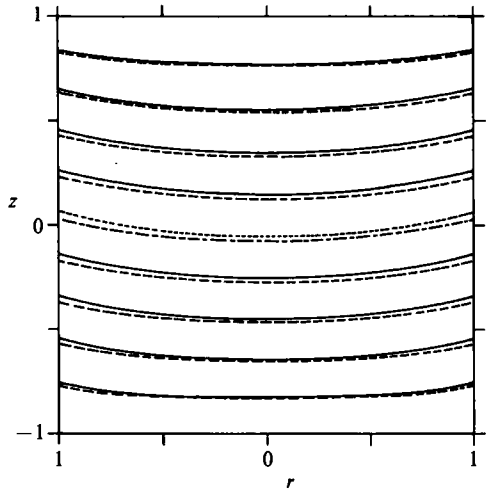

FIGURE 6. The isotherms in the interior of the liquid cylinder due to the convective effects of the motion caused by centrifugal buoyancy with $A = 1$ and $B = 0$ (——) and $B = 1$ (— — —). The parameter group $\epsilon\alpha\, Pr\, A^{-1}E^{-\frac{1}{2}}$ is set equal to one to emphasize the correction to the linear temperature profile.

where
$$Nu \equiv \frac{QL}{k\pi a^2 \Delta T}. \tag{5.5b}$$

From the previous analysis we find

$$Nu = \pm 1 - \tfrac{1}{2}\epsilon\alpha\, Pr\, E^{-\frac{1}{2}}A^{-1}F(A,B), \tag{5.6a}$$

where
$$F(A,B) = 1 - 2\sum_{n=1}^{\infty} \frac{1}{\lambda_n^2}\left[\frac{1+\dfrac{2B}{(A\lambda_n)^2}}{1+\dfrac{BI_0(A\lambda_n)}{A\lambda_n I_1(A\lambda_n)}}\right]. \tag{5.6b}$$

The function $F(A,B)$ is shown in figure 7 for various values of A. Note that when $B = 0$,

$$F = 1 - 2\sum_{n=1}^{\infty} \frac{1}{\lambda_n^2} = 0, \quad Nu = \pm 1. \tag{5.7}$$

When the Biot number is zero the imposed heat flux at the lateral boundary is exactly enough to balance the rate of internal heat generation. The temperature field given by (5.4*a*) is even, so the heat flux at both ends is either into the cylinder or out of it. Thus the only way to conserve energy when $B = 0$ is to have no heat flux at the ends, due to convection, i.e. $F(A,B) = 0$.

As B increases from zero, the net heat flux from the lateral surface is reduced because there is an increased heat flux from the ambient gas to the core given by the B^0T^1 term. This reduces the temperature difference at any z-location between the lateral surface and the ambient gas as shown in figure 6. Correspondingly the heat flux *out* of the cylinder at the ends, due to convection, must be increased an equivalent amount, and the Nusselt number, i.e. the total heat flux *into* the cylinder, decreases.

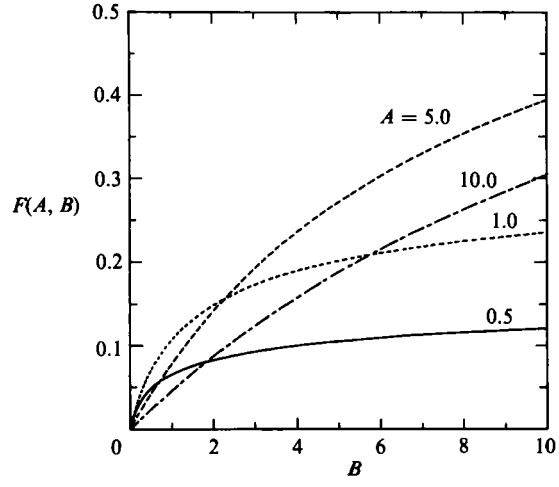

FIGURE 7. The variation of the function $F(A, B)$ defined by (5.6*b*) with the Biot number. ——, $A = 0.5$; – – – –, 1.0; — — —, 5.0; — — — — —, 10.0.

6. The first correction to the interface shape

Now that we know the flow field in the liquid cylinder due to both thermocapillarity and centrifugal buoyancy, we can compute the effects of this flow on the free-surface deformation. This can be done by considering the normal-stress boundary condition (2.3). At $O(Ca)$ we find

$$A^2S'' + (1 + B_Q)\,S = -E^{-1}p|_{r=1} + 2Au_r|_{r=1}. \tag{6.1a}$$

In addition the boundary conditions (2.1*p*, *r*) and the expansion (2.2*a*) yield at $O(Ca)$

$$S(\pm 1) = 0, \quad \int_{-1}^{1} S\,\mathrm{d}z = 0. \tag{6.1b,c}$$

6.1. *Thermocapillarity*

From the boundary-layer analysis of this problem we find that the pressure at the liquid–gas interface can be written as follows:

$$-p|_{r=1} = \frac{4^{\frac{2}{3}}E^{\frac{1}{3}}}{A^{\frac{2}{3}}} \sum_{n=1}^{\infty} \frac{(-1)^{n+1}\sin\lambda_n z}{\lambda_n^{\frac{2}{3}}} + C_1 + O(E^{\frac{1}{2}}), \tag{6.2}$$

where C_1 is a constant of integration. Since $u_r = O(1)$ we need only use the pressure term to calculate the interface shape to leading order in E.

The solution of the boundary-value problem (6.1) with the pressure term given by (6.2) is

$$S(z) = \frac{4^{\frac{2}{3}}}{A^{\frac{2}{3}}E^{\frac{2}{3}}}\left[\sum_{n=1}^{\infty} \frac{(-1)^{n+1}\sin\lambda_n z}{\lambda_n^{\frac{1}{3}}(D^2-\lambda_n^2)} - \frac{\sin Dz}{\sin D}\sum_{n=1}^{\infty}\frac{1}{\lambda_n^{\frac{1}{3}}(D^2-\lambda_n^2)}\right] + O(E^{-\frac{1}{2}}). \tag{6.3a}$$

where $D^2 = (1+B_\Omega)/A^2$. When $D = \lambda_m$, $m = 1, 2, 3, \ldots$, the solution is

$$S(z) = \frac{4^{\frac{2}{3}}}{A^{\frac{8}{3}}E^{\frac{2}{3}}}\Bigg[\sum_{\substack{n=1\\n\neq m}}^{\infty}\frac{(-1)^{n+1}\sin\lambda_n z}{\lambda_n^{\frac{5}{3}}(\lambda_m^2-\lambda_n^2)} - \frac{(-1)^{m+1}z\cos\lambda_m z}{2\lambda_m^{\frac{8}{3}}} - (-1)^{m+1}\sin\lambda_m z\sum_{\substack{n=1\\n\neq m}}^{\infty}\frac{1}{\lambda_n^{\frac{5}{3}}(\lambda_m^2-\lambda_n^2)}\Bigg] + O(E^{-\frac{1}{3}}). \quad (6.3b)$$

The interface shapes given by (6.3*a*) with $B_\Omega = 0$ and by (6.3*b*) with $B_\Omega = A^2\lambda_1^2 - 1$ are shown in figure 8. The amplitude of the deformation has been exaggerated for clarity. Equations (2.2*a*) and (6.3) show that the deformation of the interface from a cylindrical shape is given as

$$\eta - 1 = O(Ca\,A^{-\frac{8}{3}}E^{-\frac{2}{3}}). \quad (6.4)$$

The interface shape for this flow is consistent with the behaviour noted in other thermocapillary problems. The free-surface flow is downward and the resultant viscous forces drag nearby fluid downward also. To provide a return flow a pressure gradient is produced such that the pressure is greater at the bottom than at the top. This pressure distribution then produces the observed shape.

6.2. *Centrifugal buoyancy*

For this case the pressure at the liquid–gas interface is given as

$$-p|_{r=1} = \alpha E^{\frac{1}{2}}\sum_{n=1}^{\infty}\frac{(-1)^{n+1}}{\lambda_n}\sin\lambda_n z + C_2 + O(E^{\frac{2}{3}}), \quad (6.5)$$

where C_2 is a constant of integration. We also find $u_r = O(E^{\frac{1}{3}})$, so that the interface shape to leading order in E is again given by the pressure term.

Integrating the boundary-value problem, we obtain

$$S(z) = \frac{\alpha E^{-\frac{1}{2}}}{A^2}\Bigg[\sum_{n=1}^{\infty}\frac{(-1)^{n+1}\sin\lambda_n z}{\lambda_n(D^2-\lambda_n^2)} - \frac{\sin Dz}{\sin D}\sum_{n=1}^{\infty}\frac{1}{\lambda_n(D^2-\lambda_n^2)}\Bigg] + O(E^{-\frac{1}{3}}). \quad (6.6a)$$

When $D = \lambda_m$, $m = 1, 2, 3, \ldots$, the solution is

$$S(z) = \frac{\alpha E^{-\frac{1}{2}}}{A^2}\sum_{\substack{n=1\\n\neq m}}^{\infty}\frac{(-1)^{n+1}\sin\lambda_n z}{\lambda_n(\lambda_m^2-\lambda_n^2)} - \frac{(-1)^{m+1}z\cos\lambda_m z}{2\lambda_m^2} - (-1)^{m+1}\sin\lambda_m z\sum_{\substack{n=1\\n\neq m}}^{\infty}\frac{1}{\lambda_n(\lambda_m^2-\lambda_n^2)} + O(E^{-\frac{1}{3}}). \quad (6.6b)$$

The interface shapes given by (6.6*a*) with $B_\Omega = 0$ and by (6.6*b*) with $B_\Omega = A^2\lambda_1^2 - 1$ are identical with those shown in figure 8 for the previous problem to within the accuracy of the plotter. However, the actual deformation is scaled differently as

$$\eta - 1 = O(Ca\,\alpha A^{-2}E^{-\frac{1}{2}}). \quad (6.7)$$

As B_Ω is increased from zero the shape of the free surface stays qualitatively the same for both flows. For the particular value shown of $B_\Omega = A^2\lambda_1^2 - 1 = 1.4674$ the maximum deformation has increased by approximately 19.5 %. However, when there is no motion in the cylinder we know that there is a critical value of B_Ω past which the cylindrical shape loses its stability. The subject of the stability of rotating liquid cylinders *without additional interior motion* has been studied extensively by Brown & Scriven (1980). They found that the cylinder will first lose its stability to

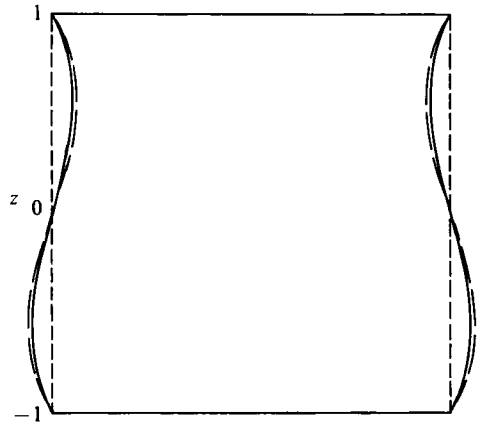

FIGURE 8. The shape of the free surface due to both the thermocapillary flow and the flow due to centrifugal buoyancy for $A = 1$, $E = 10^{-6}$, and for $B_Q = 0$ (——) and $B_Q = 1.4674$ (— — —). The amplitude of the deformation has been exaggerated for clarity.

non-axisymmetric disturbances at $B_Q = \frac{1}{4}\pi^2 = 2.4674$ when $A = 1$, but a new equilibrium shape for the liquid could not be determined. The influence of the interior motion due to thermocapillarity and centrifugal buoyancy on this free-surface instability remains a topic for future investigation.

7. Discussion

Since our initial motivation for this analysis stems from the float-zone process of crystal growth, we are especially interested in zones of silicon, one of the most common materials used in these systems. In the discussion that follows we examine whether the linear theory can be applied to the typical silicon zone described in table 1.

7.1. *The thermocapillary flow*

The linear analysis of §4 requires the nonlinear terms to be small enough to ignore. In the thermocapillary layer this restriction becomes $\epsilon A = o(E^{\frac{2}{3}})$ since we used terms up to $O(E^{\frac{2}{3}})$ in obtaining the approximation (3.8). However, the basic structure of the boundary layer is retained if $\epsilon A = o(E^{\frac{1}{3}})$. This is still a very severe restriction. Using the typical parameters for a silicon float zone from table 1, we find that

$$\Delta T \ll 0.02\ ^\circ\mathrm{C}. \tag{7.1}$$

Since a ΔT of about 20 °C is typical in an industrial silicon float zone of this size, it is obvious that the linear theory is inapplicable. Convective nonlinearities will be important in any analysis of the flow for this system. These terms could cause a thickening of the boundary layer and, possibly, a penetration into the core as the Rossby number is increased from zero.

Even though this linear theory cannot be applied to a silicon float zone, it still retains its value as an appropriate limiting case of an important industrial process. The benefits of the analysis are twofold. First, we have gained a basic knowledge of the mechanism for boundary-layer formation in a linear system. The balance of forces in the boundary layer and the range of applicability of the analysis have been identified. If this basic force balance is not disturbed very much by the influence of the convective nonlinearities, then the range of applicability of the analysis could be

much larger than predicted. The simplicity of the linear system in describing at least qualitatively the flow characteristics of the more complicated nonlinear system would then be very valuable.

Secondly, if our goal is to reduce the effects of thermocapillary convection in the core, then the linear analysis has given us an inequality with which we can guarantee a boundary-layer confinement of the flow. This inequality is of course $\epsilon A \ll E^{\frac{1}{3}}$, or equivalently,

$$\frac{\gamma_T \Delta T}{\mu \Omega a} A^2 \ll 1. \tag{7.2}$$

Even when the nonlinear terms can safely be neglected, there still remains the restriction on the Ekman number needed for the boundary-layer analysis to accurately describe the flow. Since the analysis used a power series in $E^{\frac{1}{3}}$, we must have $E^{\frac{1}{3}} \ll 1$. For the silicon float zone described in table 1, we find $E^{\frac{1}{3}} = 0.39$. Therefore we cannot expect a very accurate description of the boundary-layer flow in a silicon system when using this asymptotic analysis even when ΔT is small enough, unless Ω is increased.

Chun (1980) studied the interaction between thermocapillary convection and rotation experimentally. Here a liquid cylinder of silicone oil was heated from above with $\Delta T = 5$ °C and uniformly spun at speeds up to 1000 rev/min. At the maximum speed corresponding to $E = 0.02$ the thermocapillary motion near the axis of the cylinder was essentially suppressed, but the convective circulation was still preserved near the free surface. Thus the system showed a trend toward confinement of the thermocapillary motion near the free surface as the rotation rate increased, in agreement with the inequality (7.2). However, the velocity field in the experiment is not correctly described using this linear boundary-layer theory because the values of $E^{\frac{1}{3}} = 0.52$ and $\Delta T = 5$ °C are too large for the analysis to hold (the appropriate limits for this system are $\Delta T \ll 7.5$ °C and $E^{\frac{1}{3}} \ll 1$).

The numerical work of Kobayashi (1984) also considered the interaction of thermocapillary convection with rotation. In his model the zone was uniformly heated from the sides, so direct comparison with the present work is not possible. However, for the case of uniform rotation with $E = 0.01$ and with the other parameter values equal to those typical of a silicon float zone, he did see a confinement of the thermocapillary motion to a region near the free surface, although it was certainly too large to be called a boundary layer.

To investigate nonlinear effects the next term in the Rossby-number expansion for the thermocapillary flow could be computed. However, such a computation would be extremely difficult. In addition, the above inequalities show that in a silicon zone, at least, the nonlinear effects are not small. It seems then that the proper way to study this behaviour is either to formulate a nonlinear boundary-layer theory that could be solved numerically, or to solve the original governing equations directly as in the work of Kobayashi (1984).

7.2. *The centrifugal-buoyancy flow*

The linear theory accurately describes the centrifugal flow field when $\epsilon\alpha = \beta \Delta T \ll E^{\frac{1}{3}}$. For our typical silicon float zone described in table 1 this condition yields

$$\Delta T \ll 414 \text{ °C}, \tag{7.3}$$

which is certainly met for any zone of industrial interest.

The magnitude of the centrifugal flow field compared with the thermocapillary flow field is given by the parameter

$$A^{-1}\alpha = \frac{\rho^{\frac{1}{3}}\mu^{\frac{2}{3}}(\Omega a)^{\frac{4}{3}}\beta}{A^2\gamma_T}, \tag{7.4}$$

where α is evaluated using the thermocapillary velocity scale (3.5). For our typical silicon float zone $A^{-1}\alpha = 0.19 \times 10^{-4} \ll 1$. Thus the flow in the side layer will be dominated by the thermocapillary motion, but in the core there will be a very small motion due to centrifugal buoyancy.

7.3. *The temperature correction in the core*

The first-order temperature correction to the linear temperature profile is $O(\epsilon\alpha\, Pr\, A^{-1}E^{-\frac{1}{2}})$. This correction is solely the result of the motion due to centrifugal buoyancy and it is of the same order as that found by Homsy & Hudson (1969) for a rigid cylinder. The thermocapillary motion has no effect on the temperature in the core because it induces no interior convective motions and produces no equivalent heat fluxes on the lateral surface of the core.

For our typical silicon float zone $\epsilon\alpha\, Pr\, A^{-1}E^{-\frac{1}{2}} = 0.56 \times 10^{-4}\,\Delta T$. Even for ΔT as large as 100 °C this effect will be very small.

7.4. *The free-surface deformation*

The free-surface deformation from a cylindrical shape has been described as an expansion in powers of the capillary number. From (6.4) we see that the result for the thermocapillary flow is valid when

$$Ca \ll A^{\frac{4}{3}}E^{\frac{4}{3}}. \tag{7.5}$$

With our silicon float zone this becomes $Ca \ll 0.023$, or

$$\Delta T \ll 254\ ^\circ\text{C}. \tag{7.6}$$

This restriction is certainly met when the flow can be described by the linear theory, so in this case the liquid stays cylindrical to first order. However, in those situations in which the linear theory is invalid the result (7.5) is also invalid since it is based on a pressure field obtained from the linear theory. When nonlinear effects are appreciable the pressure could increase and the normal stresses on the free surface could become comparable to the surface-tension forces resulting in significant surface deflections. Therefore the non-deformability assumption can only be justified on the basis of a full nonlinear calculation.

The surface deflection calculated for the flow due to centrifugal buoyancy is valid when

$$Ca \ll \alpha^{-1}A^2E^{\frac{1}{2}}. \tag{7.7}$$

For our silicon zone this is $Ca \ll 3100$, or

$$\Delta T \ll 3.4 \times 10^7\ ^\circ\text{C}. \tag{7.8}$$

Thus we see that linear theory adequately describes both the flow and the deformation of the free surface in this case.

8. Conclusions

Both experimental and numerical work has indicated that a large enough uniform rotation of a float zone would tend to confine the thermocapillary motion to a region near the free surface. This observation provided the motivation to calculate the flow

field in the rapid rotation limit. To begin, we developed a linear theory using the standard techniques for rotating flows as discussed by Greenspan (1968). However, we departed from common practice when we solved for the flow using a multiscale perturbation method. This method enabled us to obtain a first-order correction to the thermocapillary flow that is uniformly valid in the radial coordinate. For completeness, we also calculated the flow field and the correction to the temperature field in the core due to centrifugal buoyancy, and the deformation of the interface shape for both of the above flows. The interesting new features exhibited by this system are the free-surface velocity scale given by (3.5) and the free-surface deflection scales given by (6.4) and (6.7).

The linear theory also yielded explicit inequalities which determined when the theory was applicable to a particular system. Unfortunately, these relations show that the thermocapillary motion in a small silicon zone, which is of particular interest to crystal growers, is not governed by the linear theory. In fact, nonlinear effects seem to be very important for this case. Thus further investigation into the nonlinear structure of the confined region in a rapidly rotating float zone is warranted.

The author would like to thank Professor H. P. Greenspan for many helpful discussions during the course of this work, and Drs W. W. Fowlis and D. O. Roberts for their comments on an earlier version of this paper.

This work was supported in part by the National Aeronautics and Space Administration, Materials-Processing-in-Space-Program, Contract NAS8-35412 and by the North Atlantic Treaty Organization under Grant NATO-1982.

REFERENCES

Barcilon, V. & Pedlosky, J. 1967 *J. Fluid Mech.* **29**, 673.

Brown, R. A. & Scriven, L. E. 1980 *Phil. Trans. R. Soc. Lond.* A **297**, 51.

Chun, C.-H. 1980 *J. Cryst. Growth* **48**, 600.

Greenspan, H. P. 1968 *The Theory of Rotating Fluids.* Cambridge University Press.

Homsy, G. M. & Hudson, J. L. 1969 *J. Fluid Mech.* **35**, 33.

Hunter, C. 1967 *J. Fluid Mech.* **27**, 753.

Keller, W. & Muhlbauer, A. 1981 In *Floating-Zone Silicon; Preparation and Properties of Solid State Materials*, vol. 5 (ed. W. R. Wilcox). Marcel Dekker.

Kobayashi, N. 1984 *J. Cryst. Growth* **66**, 63.

Schwabe, D. 1981 *Physico-Chem. Hydrodyn.* **2**, 263.

Schwabe, D., Scharmann, A., Preisser, F. & Oeder, R. 1978 *J. Cryst. Growth* **43**, 305.